BULLETIN OF THE POLISH ACADEMY OF SCIENCES
TECHNICAL SCIENCES
DOI: 10.24425/bpasts.2025.153829

THIS IS AN EARLY ACCESS ARTICLE.
This article has been accepted for publication in a future issue of this journal, but has not been fully edited. Content may change prior to final publication.

# Handling stability analysis of decoupling suspension for formula racing

**Han Xu[1], Jiachuan Xu[1], Xuemin Cui[1], Yang Zhou[1], Xinyu Sun[1], and Zongqi Wang[1]**

[1] Shandong University of Technology, China

**Abstract..** In this paper, a university formula racing suspension is taken as the research object. Based on the requirements of racing suspension, the double wishbone suspension is improved, and a new arrangement scheme based on the stepped shaft is proposed, which theoretically realizes the decoupling of the pitch stiffness and the roll stiffness of the suspension. Based on ADAMS/Car module, the front and rear suspension models are established. By simulating the motion of formula racing, it is further judged whether the pitch and roll stiffness of the suspension are decoupled. According to this, the hard point coordinates of the suspension is adjusted to ensure that the length of each spring changes within the ideal range. Based on the optimized suspension, according to the national standard test method and the scoring standard of the automobile industry, combined with the university formula racing project, the vehicle handling stability test and scoring evaluation are carried out, and the vehicle handling stability is verified by the real vehicle test. A set of decoupling suspension is obtained, which can realize separate adjustment of pitch stiffness and roll stiffness and improve vehicle handling stability.

**Key words:** decoupling suspension; ADAMS/CAR; formula racing

## 1. INTRODUCTION

Formula SAE of China (FSAE) is a car design and manufacturing event. The main participants are college students majoring in vehicle engineering and related fields. The participating teams are all composed of schools as units. Additionally, with the rapid development of the university formula racing competition, people have increasingly high requirements for the handling stability of the racing[1-3]. Most domestic and foreign fleets adopt the conventional suspension with double shock absorbers and lateral stabilizer bars, and the pitch and roll solution of the suspension is realized by adding a third spring or a lateral stabilizer bar[4-5]. However, the adjustable upper limit of scheme suspension is relatively low, and the suspension mass is significantly increased, which is not conducive to improving the handling stability of the racing.

When the suspension pitch stiffness and roll stiffness of the racing are provided by the main springs on both sides, To improve the steady-state steering characteristics of the racing, the spring stiffness needs to be increased to improve the roll stiffness, but at this time, the pitch stiffness increases, resulting in poor ride comfort; Conversely, when the ride comfort is improved by reducing the spring stiffness to reduce the pitch stiffness, the roll stiffness is reduced, making the racing steering characteristics worse.

To improve the suspension angle stiffness without affecting the suspension line stiffness, R Sindhwani et al. validated that anti-roll bars can reduce the amplitude of body roll during wheel turns and improve the racing stability[6]; Y Kumar et al. studied that adding anti-roll bars in suspension systems reduces the change in camber angle, which can better control cornering[7]. I JAVANSHIR et al. minimize suspension system camber angle variations by adding anti-roll bars and optimising torsion bars[8]. Kelkar S et al. investigated the importance of an anti-roll bar device to tune the roll stifness of the car without interfering with the ride stifness[9]. Ke Ma added lateral stabilizer bars to the front and rear air suspension systems. The results show that the comprehensive evaluation score of handling stability increased from 80.38 to 85.05, and the handling stability of the full vehicle was improved[10]. To decouple suspension line stiffness and angular stiffness, some scholars have proposed adding a third spring to provide additional line stiffness. Liu Z et al. explained the geometric design of the racing suspension and the calculation process of the stiffness of each spring after adding the third spring[11]; Shi X, et al. studied the working principle of adding a third spring and conducted kinematic simulation[12]. Yang S et al. of Wenzhou University designed a three-spring decoupling suspension to realize the decoupling of suspension and adjust the pitch stiffness and roll stiffness separately[13]. On the basis of the double wishbone non-independent suspension, Dongmei Wu et al. changed the hard point design of the spring position, and adopted the geometric suspension layout form of one spring transversely placed and one spring oblique placed, so as to realize the decoupling between the roll motion and pitch motion of the formula racing[14]. Shuanglu Quan, et al. connected the rotating centers of the two shock absorbers to the frame through bearings, and rotated the rotating shaft through

*e-mail: xujc@sdut.edu.cn



This article has been accepted for publication in a future issue of this journal, but has not been fully edited. Content may change prior to final publication.

the push rod, so as to compress the shock absorber and inhibit the tendency of vehicle trim. Realize the decoupling of suspension pitch stiffness and roll stiffness[15].

Through the above analysis, the adjustable property of double shock absorber and side stabilizer bar suspension is limited and the mass is increased, the third spring design cannot completely realize the decoupling of pitch and roll stiffness, and some decoupling suspensions designed by some scholars lack of full vehicle simulation and real vehicle test, and the improvement of vehicle handling stability by such design is to be verified. Therefore, a decoupling suspension design scheme is proposed in this paper. Two independent spring shock absorbers correspond to the trim and roll conditions respectively, theoretically realizing the decoupled pitch stiffness and roll stiffness. Based on ADAMS/Car module, a suspension dynamic model is established for simulation and optimization to verify the correctness of theoretical analysis. Finally, a real vehicle test is carried out to verify the improvement of handling stability of the full vehicle by the design.

To determine the impact of suspension on the handling and stability performance of the racing, most scholars use virtual simulation to study the overall performance of the racing[16]. A Pridie and C Antonya designed a formula racing suspension and conducted braking and acceleration simulation tests on the virtual model[17]. Zhang L et al. according to the evaluation index of minimum time handling and stability, the vehicle performance was analyzed and contrasted by ADAMS/CAR[18]. B M Kim et al. established a virtual prototype model of the suspension of a heavy truck. The key hard point coordinates of the suspension are taken as the design variables to optimize the suspension characteristics[19]. To improve the suspension performance of the racing, T Vlad et al. optimized the wheel alignment parameters by identifying hard point coordinates that had a large impact on the optimization objectives[20]. Zhang Z et al. conducted a simulation of the vehicle dynamics model of the racing in the Eight-shaped ring project, analyzing the performance of the racing on actual tracks[21]. M Balena et al. conducted an acceleration, braking, and Eight-shaped ring project on the racing dynamics model to assess the overall handling stability of the racing[22]. However, there are certain subjective factors in the evaluation parameters of the test, which cannot better evaluate the overall performance of the racing.

To judge more objectively whether the relevant parameters of each test of the racing meet the requirements, most researchers refer to the Chinese vehicle handling stability test method to conduct simulation tests and evaluate according to the Chinese vehicle handling stability index limit and evaluation method[23-24]. Chai Y conducts kinetic simulation optimization on FSAE racing suspension based on ADAMS/CAR software, and carries out vehicle handling stability simulation and score evaluation[25]; Zhang H conducted simulation tests such as steady-state slewing test and snake-shaped test on FSAE racing and scored and evaluated each evaluation parameter[26]. The relevant researchers refer to the Chinese test method to test the FSAE racing, but the radius of the Steady-state slewing test and the pile spacing of the snake-shaped test are greater than the radius and pile spacing of the racing competition project. The score obtained by the test can show that the vehicle meets the competition requirements, but the competition performance cannot be better judged.

To better judge the performance of the racing, Zhou D from Chang'an University proposed an index to evaluate the Steady-state slewing test, i.e., the maximum lateral acceleration[27]. Large lateral acceleration means that the lateral limit performance of the vehicle is better, and the control stability of the full vehicle is also better; Qiao J et al. from Chang'an University pointed out that racing with a large lateral acceleration can quickly pass through the splayed loop project with a turning radius of only 9.125m[28]. Therefore, the maximum lateral acceleration is taken as the evaluation index of the Steady-state slewing test; Yang C and Hong C proposed taking the maximum lateral acceleration as the evaluation index of the Steady-state slewing test and determined the upper and lower limits of the scoring formula according to the results[29-30].

The above analysis has reference significance for the handling stability evaluation of formula racing. This paper comprehensively considers the test methods of national standards, industry evaluation standards and competition project requirements, and uses the maximum lateral acceleration, understeer degree and body roll degree as the evaluation indicators of the test. In addition, the test standards and difficulties are improved, and the comprehensive score of the Steady-state slewing test is calculated, so as to evaluate the vehicle handling stability more comprehensively.

## 2. Decoupled Suspension Scheme and Design

The decoupled layout scheme is adopted for the suspension to solve the problem of pitch stiffness and roll stiffness being difficult to adjust, and the motion law of the suspension is analyzed. The workflow is shown in Fig. 1.

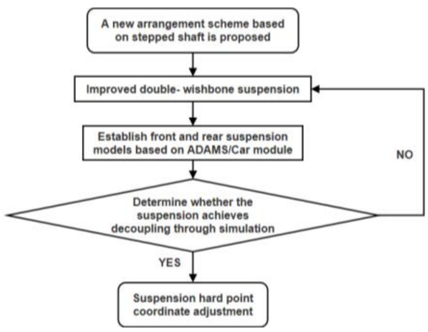


Design and verification of decoupling suspension

**Fig.1.** Workflow Diagram 1

### 2.1. Dynamic analysis of decoupling suspension layout scheme

(1) Layout scheme

The main components and arrangement scheme of decoupling suspension are shown in Fig. 2 Due to the approximate horizontal arrangement of the shock absorber in the FSAE racing suspension design, the small ground clearance of the racing, and the low height of the whole vehicle, the rocker arm required for the connection between the shock absorber and the cross-arm is transformed into a stepped shaft, as shown in Fig. 2 (a) and (b). There are two rotating arms on one stepped shaft,



This article has been accepted for publication in a future issue of this journal, but has not been fully edited. Content may change prior to final publication.

and the connection points on the rotating arm are respectively connected with the push rod and two spring shock absorber assemblies. Both ends of the stepped shaft are fixed on the frame through the support.

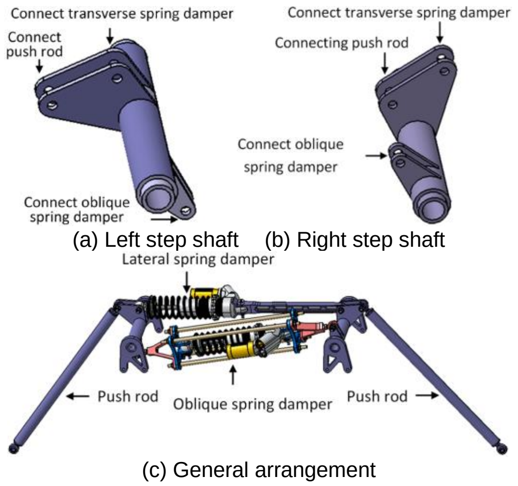


**Fig.2.** Decoupling arrangement

(2) Analysis of motion

When the racing is in pitch motion, push rods on both sides push the step shaft and rotate inward simultaneously. The distance between the two points connecting the lateral spring damper assembly on the ladder shafts on both sides becomes shorter. Therefore, the lateral spring damper assembly is compressed. While the step axis rotates inward simultaneously, the distance between the two points connecting the inclined spring damper assembly on the ladder shafts on both sides remains the same. Therefore, the inclined spring damper assembly is not compressed, as shown in Fig. 3(a).

When the racing is in roll motion, push rods on both sides push the ladder shaft to rotate clockwise or counterclockwise simultaneously. The distance between the two points connecting the lateral spring damper assembly on the ladder shafts on both sides remains the same. Therefore, the lateral spring damper assembly is not compressed or extended. While the step shaft rotates clockwise or counterclockwise simultaneously, the distance between the two points connecting the inclined spring damper assembly on the ladder shafts on both sides becomes longer or shorter. Therefore, the inclined spring damper assembly is compressed or stretched, as shown in Fig. 3(b).

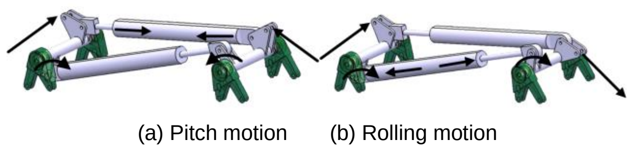


**Fig.3.** Motion law of decoupling suspension

It can be seen from motion analysis the length of the inclined spring damper assembly remains the same when the racing body is in pitching motion. The length of the lateral spring damper assembly remains the same when the racing body rolls, so the lateral springs provide the pitch stiffness of the suspension, and the inclined springs provide the roll stiffness of the suspension; decoupling of suspension pitch stiffness and roll stiffness is theoretically realized.

### 2.2. Modeling and Simulation Analysis of Decoupling Suspension

The decoupling suspension model is established in the ADAMS/CAR module and assembled with the suspension test bench to obtain the simulation models of front and rear suspension test benches, as shown in Fig. 4.

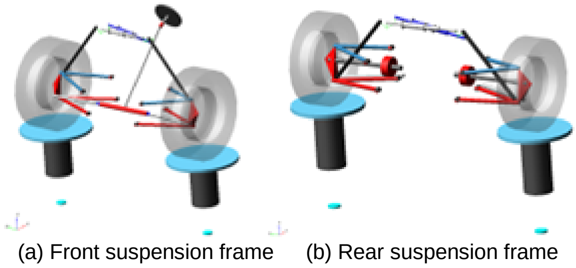


**Fig.4.** Simulation model

The simulation of suspension is realized by inputting excitation to wheels. Input the vertical run-out of the same size and direction to the left and right wheels of the same axle to simulate the wheel run-out caused by the car body when encountering obstacles or accelerating and decelerating; Enter the same but opposite vertical run-out to simulate the wheel run-out caused by the car turning. The lateral spring provides rigidity under the excitation of two wheels in the same direction. If the oblique spring does not work, the change of its length shall be as small as possible. Under the double-wheel reverse excitation, the inclined spring provides rigidity, the horizontal spring does not work, and the change of its length is as small as possible.

To further judge whether the decoupled suspension is completely decoupled, the front and rear suspensions are input with the excitation of two wheels in the same direction and the excitation of two wheels in the opposite direction. The wheel run-out range is [- 30mm, 30mm]. Observe the spring length change that does not provide rigidity when the front and rear suspensions are jumping, and optimize and adjust the hard point coordinates of the suspension according to the simulation results. Through continuous iterative calculation, the final spring length change curve that does not provide the rigidity is obtained, as shown in Fig. 5 and Fig. 6.

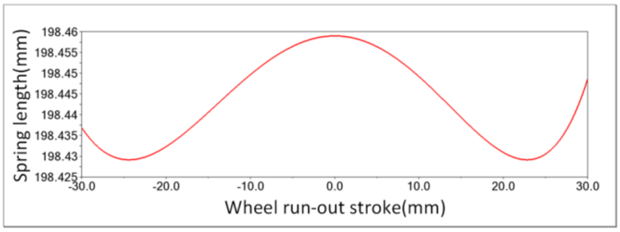


(a) Length of oblique spring when the double wheels bounce in the same direction

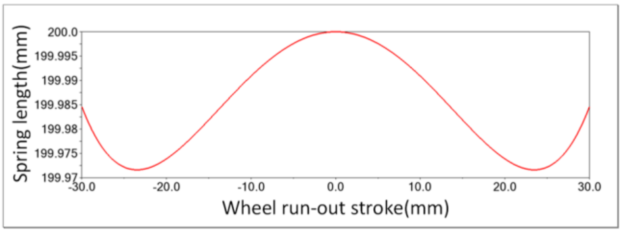


(b) Length of lateral spring when the double wheels bounce in the opposite direction

**Fig.5.** Simulation curve of length change of front suspension spring



This article has been accepted for publication in a future issue of this journal, but has not been fully edited. Content may change prior to final publication.

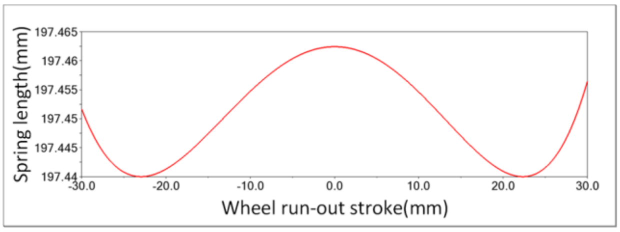


(a) Length of oblique spring when the double wheels bounce in the same direction

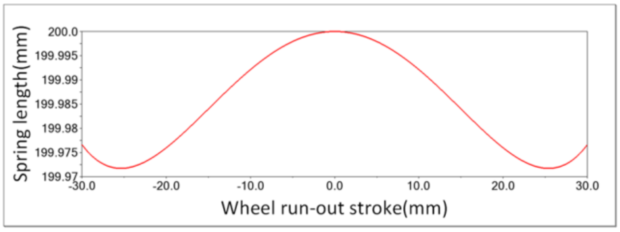


(b) Length of lateral spring when the double wheels bounce in the opposite direction

**Fig.6.** Simulation curve of length change of rear suspension **spring**

It can be seen from Fig. 5 that the length variation of the front suspension inclined spring is 0.06mm under the excitation of double wheels in the same direction. Under the opposite direction excitation of double wheels, the length variation of the transversal spring is 0.04mm, and the length variation of the spring is minimal.

It can be seen from Fig. 6 that the length variation of the inclined spring of the rear suspension is 0.04mm under the excitation of double wheels in the same direction. Under the opposite direction excitation of double wheels, the length variation of the transversal spring is 0.06mm, and the length variation of the spring is minimal.

Through analysis, it can be seen that the length change of the oblique spring is small under the same direction of double-wheel excitation, and the length change of the lateral spring is small under the opposite direction of double-wheel excitation. However, the wheel run-out in the actual competition is far less than the tire run-out simulated by simulation, so the spring not providing the stiffness has a small change, which realizes the decoupling of pitch stiffness and roll stiffness.

### 2.3. Wheel Alignment Parameter Selection and Suspension Geometry Design

Based on the simulation results and the competition experience over the years, select the wheel positioning parameters[31] and design the hard point size of the suspension geometry.

(1) Selection of wheel alignment parameters

Wheel alignment parameters mainly include camber angle, toe-in angle, kingpin inclination angle, and kingpin caster angle. Wheel alignment parameters as shown in Table 1.

(2) Suspension geometry design

Based on the simulation results and the entry experience of Shandong University of Technology in formula racing, the basic parameters for setting the suspension design are shown in Table 2.

The front view of the front suspension is designed according to the geometric design knowledge of the vehicle suspension, as shown in Fig. 7.

Hard point coordinates of front and rear suspensions are shown in Table 3 and Table 4.

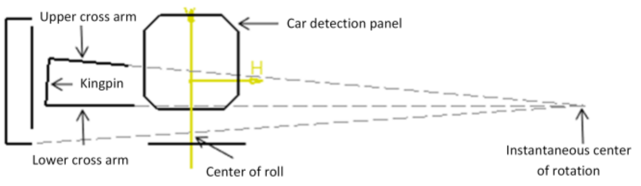


**Fig.7.** Front view geometry of the front suspension

**TABLE 1.** Wheel alignment parameters

| Positioning parameters | Camber angle | Toe-in Angle | Kingpin caster angle | Kingpin inclination angle |
|---|---|---|---|---|
| Front suspension frame | -1° | -0.2° | 3.52° | 4° |
| Rear suspension frame | -1° | 0.1° | 0 | 0 |

**TABLE 2.** Basic parameters

| Wheelbase (mm) | Wheel track(mm) | Axle load ratio | Cross arm ratio | Offset frequency (Hz) | Height of center of mass(mm) |
|---|---|---|---|---|---|
| 1560 | 1180 | 47:53 | 0.8 | 3.6 | 320 |

**TABLE 3.** Coordinate of initial hard point of front suspension

| Name | | X | Y | Z |
|---|---|---|---|---|
| hpl_bc | Forward point of step axis | 90.765 | -180 | 420 |
| hpl_bc2 | Rear point of step axis | 10.765 | -180 | 420 |
| hpl_lca_front | Front point of lower wishbone | -150 | -200 | -88.075 |
| hpl_lca_outer | Outer point of lower wishbone | 0 | -549 | -92 |
| hpl_lca_rear | Rear point of lower wishbone | 150 | -200 | -88.075 |
| hpl_prod_inboard | Push rod inner point | 10.765 | -215.3 | 454.8 |
| hpl_prod_outboard | External point of push rod | 10.765 | -501.763 | 100 |
| hpl_tierod_inner | Inner point of steering tie rod | -29.0031 | -219.933 | -61.7 |
| hpl_tierod_outer | Outer point of steering tie rod | -58.579 | -545 | -57.53 |
| hpl_uca_front | Front point of upper wishbone | 139.235 | -240.77 | 50.231 |
| hpl_uca_outer | Outer point of upper wishbone | 10.765 | -536.763 | 83 |
| hpl_uca_rear | Rear point of upper wishbone | 160.765 | -240.77 | 50.231 |
| hpl_wheel_center | Wheel core point | 0 | -595 | 0 |
| hps_roll_1 | Left point of oblique spring damper | 90.765 | -172 | 387.7 |



This article has been accepted for publication in a future issue of this journal, but has not been fully edited. Content may change prior to final publication.

| | | | | |
|---|---|---|---|---|
| hps_roll_2 | Right point of oblique spring damper | 90.765 | 172 | 454.4 |
| hps_trim_left.y | Left point of lateral spring damper | 10.765 | -172.9 | 452 |
| hps_trim_right.y | Right point of lateral spring damper | 10.765 | 172.9 | 452 |

**TABLE 4.** Coordinate of initial hard point of rear suspension

| Name | | X | Y | Z |
|---|---|---|---|---|
| hpl_bc | Forward point of step axis | 1605 | -200 | 210 |
| hpl_bc2 | Rear point of step axis | 1525 | -200 | 210 |
| hpl_drive_shaft_inr | Drive axle shaft output point | 1560 | -200.66 | 0 |
| hpl_lca_front | Front point of lower wishbone | 1450 | -225.23 | -86.621 |
| hpl_lca_outer | Outer point of lower wishbone | 1525 | -523 | -93 |
| hpl_lca_rear | Rear point of lower wishbone | 1640 | -225.23 | -86.621 |
| hpl_prod_inboard | Push rod inner point | 1525 | -235 | 240 |
| hpl_prod_outboard | External point of push rod | 1525 | -500 | -73 |
| hpl_tierod_inner | Inner point of lower pull rod | 1690 | -225.23 | -86.621 |
| hpl_tierod_outer | Outer point of lower pull rod | 1575 | -523 | -93 |
| hpl_uca_front | Front point of upper wishbone | 1440 | -270.32 | 57.559 |
| hpl_uca_outer | Outer point of upper wishbone | 1555 | -517.098 | 76 |
| hpl_uca_rear | Rear point of upper wishbone | 1670 | -270.32 | 57.559 |
| hpl_wheel_center | Wheel core point | 1560 | -585 | 0 |
| hps_roll_1 | Left point of oblique spring damper | 1605 | -195.4 | 175.4 |
| hps_roll_2 | Right point of oblique spring damper | 1605 | 195.4 | 242.6 |
| hps_trim_left | Left point of lateral spring damper | 1525 | -199.5 | 242.8 |
| hps_trim_right | Right point of lateral spring damper | 1525 | 199.5 | 242.8 |

## 3. Establishment of Full vehicle model

Based on the ADAMS/CAR module, the assembly models of front suspension, steering, tire, body, power, and brake subsystem are simulated and analyzed to reflect the racing performance in actual operation better.

### 3.1. Steering Subsystem.

A rack-and-pinion steering system is adopted for the racing. ADAMS/CAR software's steering system template is adopted. Set the rack angular transmission ratio as 0.078rad/m, modify corresponding parameters, adjust each node's hard point coordinates, and generate the steering subsystem based on the template in the standard mode.

### 3.2. Tire Subsystem.

The tires used by Shandong University of Technology every year are Hoosier hot-melt tyres, which have a great grip. The tire system template of ADAMS/CAR software is used to modify the tire geometry and relevant parameters and generate the tire subsystem based on the template.

### 3.3. Body subsystem.

In the actual body system, there are many mechanical parts, the establishment of the model is more complex, and the complex vehicle body system is simplified into a spherical object. This paper mainly studies the influence of suspension systems on vehicle handling stability, so the influence of air on the kinematic model is ignored. The spherical automobile body subsystem of ADAMS/CAR software is adopted. It adds vehicle body location information, quality information, communicator information, etc., and generates the vehicle body subsystem based on the template.

### 3.4. Power assembly and brake subsystem.

In ADAMS/CAR software, the power system is different from other models because there is no need to establish a real model; instead, external characteristic curve of an engine of the racing and transmission ratios at all levels of the transmission are edited into the property file of the power module in the setting, data, and mathematical functions simulate the powertrain to drive the vehicle movement. The brake system is also set by setting parameters such as braking force and friction area.

### 3.5. Full vehicle model.

In Standard mode, each subsystem is assembled into a full vehicle simulation model through assembly and test stand, as shown in Fig. 8 To properly match the suspension with the vehicle, obtaining the racing vehicle parameters is necessary. The vehicle parameters measured are shown in Table 5.

**TABLE 5.** Basic parameters of full vehicle

| Parameter name | Parameter value | Parameter name | Parameter value |
|---|---|---|---|
| Total length(mm) | 3001 | Curb weight(kg) | 240 |
| Total Width(mm) | 1417 | Quality of driver(kg) | 70 |
| Total height(mm) | 1190 | Height of center of mass(mm) | 300 |
| Wheelbase (mm) | 1580 | Axle load ratio | 47:53 |
| Front wheel track(mm) | 1190 | Distance between center of mass and front axle(mm) | 826.8 |
| Rear wheel track(mm) | 1170 | Distance between center of mass and rear axle(mm) | 733.2 |


This article has been accepted for publication in a future issue of this journal, but has not been fully edited. Content may change prior to final publication.

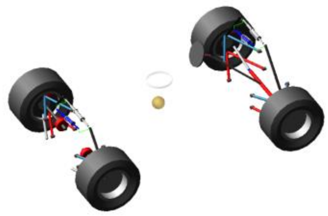

**Fig.8.** Full vehicle model

## 4. Simulation And Evaluation of Vehicle Handling Stability Test

By GB/T6326-2014 Automobile Handling Stability Test Method (2014) and QC/T 480-1999 Limits and Evaluation Methods of Automobile Handling Stability Index (1999) and in combination with the University Formula Racing Project, the vehicle is subjected to the Steady-state slewing test, snaking test and scoring evaluation. The workflow is shown in Fig. 9.

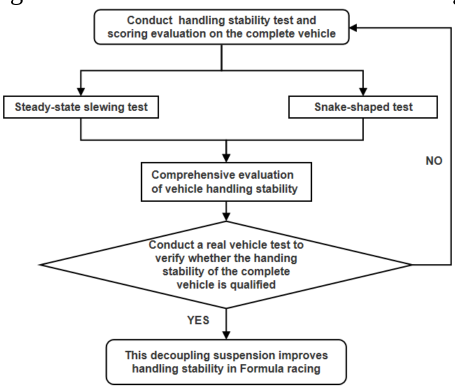


Simulation And Evaluation of Vehicle Handling Stability Test
**Fig.9.** Workflow Diagram 2

### 4.1. Steady-state slewing test.

The Steady-state slewing test mainly tests the stability and control performance of the vehicle and analyzes whether the car is stable under the steering input.

The figure of Eight-shaped ring project in FSAE competition is similar to the steady-state slewing test, but its turning radius is far less than 15m in the national standard steady-state slewing test. In this paper, according to the national standard and the actual situation of FSAE race, the steady-state slewing test of the car is carried out, so that the car runs along a circle with a radius of 9.125m. Therefore, the final score of the steady-state slewing test is lower than that of the test with a radius of 15m.

(1) Steady-state slewing test method

The racing runs at 10km/h (minimum stable speed) along the circumference with radius of 9.125m. The vehicle is driven along the circumference by continuously adjusting the steering wheel angle, and the speed is gradually increased until the maximum lateral acceleration is reached (the maximum lateral acceleration of the vehicle is 1.03g through multiple tests). The whole test process is recorded.

(2) Steady-state slewing test setup and simulation results

In the vehicle simulation of ADAMS/CAR software module, select the turning test with the radius unchanged, set relevant parameters according to the test method, and allow the vehicle to shift gears. The simulation duration is 15s, and the simulation path is shown in Fig. 10.

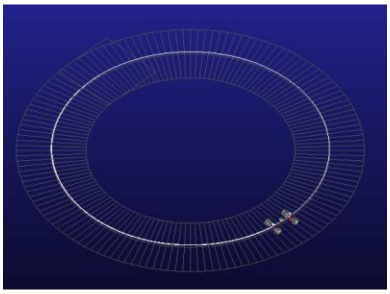

**Fig.10.** Roadmap of Steady-state slewing test track

Fig. 11(a)-(c) shows the Steady-state slewing test simulation results. Based on the test data, the relation curve between the steering wheel angle, the difference between the front and rear axle lateral deflection angles, and the lateral acceleration of the body can be obtained, as shown in Fig. 11(d)-(f), it provides the basis for the corresponding scoring evaluation formula.

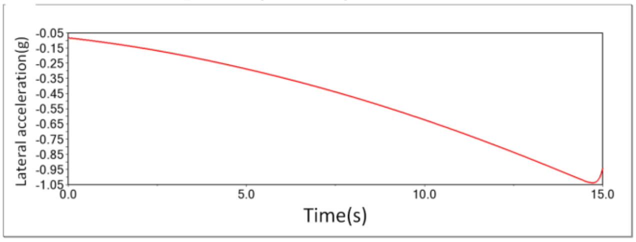


(a) Lateral acceleration variation curve

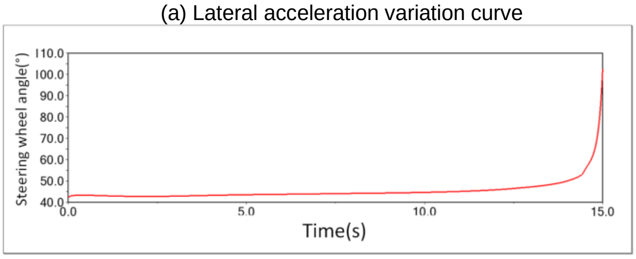


(b) Steering wheel angle change curve

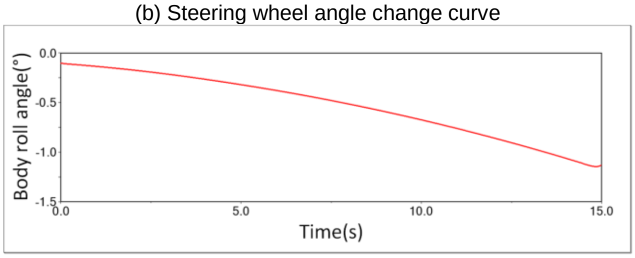


(c) Change curve of body roll angle

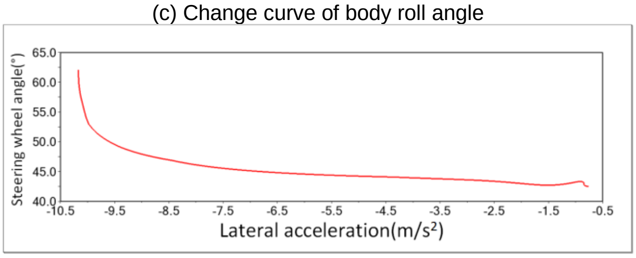


(d) Relation curve between steering wheel angle and lateral acceleration

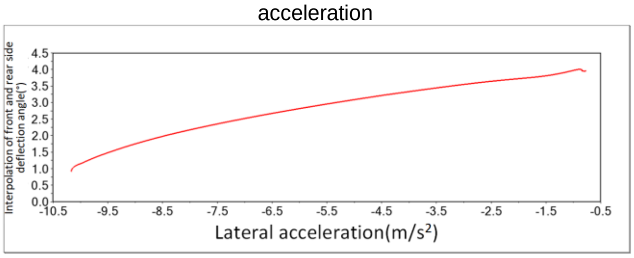


(e) Relation curve between front and rear lateral deflection angle difference and lateral acceleration


This article has been accepted for publication in a future issue of this journal, but has not been fully edited. Content may change prior to final publication.

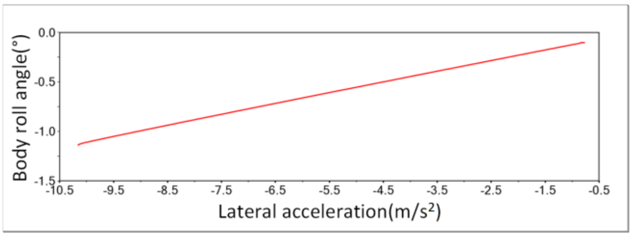


(f) Relation curve between body roll angle and lateral acceleration

**Fig.11.** Simulation curve of steady-state rotation test

Fig. 11(d) shows that the lateral acceleration increases from -0.9m/s2 to -9.7m/s2. To maintain a pre-determined path, the steering angle is increased by 7.4 °, and the racing shows a slightly understeer. At present, most cars pass through various curves quickly Toto improve the vehicle's handling flexibility, and the steering characteristics are designed to be slightly understeer.

(3) Scoring evaluation of Steady-state slewing test

Due to the small turning radius and track width of the Eight-shaped ring project in FSAE racing events, the vehicles participating in the event need to have a large lateral acceleration to improve the sensitivity of the racing when turning, to pass through the curve at a higher stable speed. In the evaluation method of automobile industry standard, the lateral acceleration of neutral steering point is one of the evaluation indicators of Steady-state slewing test [12]. However, the car has a slightly understeer characteristic with no neutral point. Based on the evaluation method of automobile industry standard, in this case, the least square method shall be adopted, and the calculation shall be carried out according to the cubic polynomial fitting curve of the variable term. The calculated side acceleration score for neutral steering is full, but cars need a greater side acceleration to improve the race.

Therefore, the maximum lateral acceleration is taken as one of the evaluation indicators of the test. The understeer degree and the body roll degree are scored according to the automobile industry standard, and the comprehensive score is finally calculated.

1 Maximum lateral acceleration score

Calculation formula of maximum lateral acceleration score:

$$N_{a_n} = 60 + \frac{40}{a_{100} - a_{60}} \left(a - a_{60}\right) \tag{1}$$

Where, $N_{a_n}$ is the evaluation score of maximum lateral acceleration, $a$ is the test value of maximum lateral acceleration; $a_{60}$, $a_{100}$ Respectively the lower limit and upper limit of maximum lateral acceleration.

$a_{60}$ and $a_{100}$ are determined according to previous FSAE racing results, $a_{60}$ is 0.9g, $a_{100}$ is 1.4g. From Fig. 11(a), it can be seen that the maximum lateral acceleration $a$ is 1.03g. Substitute each parameter into Eq. (1) to obtain the evaluation score $N_{a_n}$ =70.4 of the maximum lateral acceleration of the Steady-state slewing test.

2 Scoring of understeer

The formula for calculating the understeer score is:

$$N_U = 60 + \frac{U\left(U_{60} - U\right)\left(\lambda - U\right)}{U_{100}\left(U_{60} - U_{100}\right)\left(\lambda - U_{100}\right)} \times 40 \tag{2}$$

Where, $N_U$ is the evaluation score of the understeer degree; $U$ is the test value of insufficient steering degree; is the coefficient calculated by the ratio of to $U_{100}$ , $\lambda = \frac{2 \times U_{60} / U_{100}}{U_{60} / U_{100} - 2}$ ; $U_{60}$ and $U_{100}$ are the lower and upper limits of understeer respectively. $U_{100}$ =0.4(°)/(m/s$^2$), $U_{60}$ =1.0(°)/(m/s$^2$).

As shown in Fig. 11(e), the insufficient steering angle $U$ =0.15 (°)/(m/s$^2$). Substituting each parameter into Eq. (2) yields an evaluation score of $N_U$ =81.8 for insufficient steering degree.

3 Body roll rating

The calculation formula of car body roll degree score is:

$$N_\phi = 60 + \frac{40}{K_{\phi 60} - K_{\phi 100}} \times \left(K_{\phi 60} - K_\phi\right) \tag{3}$$

Where, $N_\phi$ is the evaluation score of car body roll, $K_\phi$ is the test value of car body inclination, $K_{\phi 60}$ and $K_{\phi 100}$ are the lower and upper limits of the body roll. $K_{\phi 100}$ =0.7(°)/(m/s$^2$), $K_{\phi 60}$ =1.2(°)/(m/s$^2$).

It can be seen from Fig. 11(f) that the body roll $K_\phi$ is 0.11 (°)/(m/ s$^2$). Substitute each parameter into Eq. (3) to obtain the evaluation score $N_\phi$ =147.2.

When the evaluation score exceeds 100, the comprehensive score is calculated as 100, so $N_\phi$ =100.

4 Comprehensive scoring of Steady-state slewing test

The formula for calculating the comprehensive score of the Steady-state slewing test is:

$$N_W = \frac{N_{a_n} + N_U + N_\phi}{3} \tag{4}$$

Substitute each parameter into Eq. (4) to obtain the comprehensive score $N_W$ =84.1 for the steady-state slewing test.

The Steady-state slewing simulation curve and test score show that the body roll score is high and the understeer degree also meets the requirements. The final score of the Steady-state slewing test is 84.1.

### 4.2. Snake-shaped test.

The snake-shaped test, also known as the S-shaped pile winding test, makes the vehicle continuously simulate the Serpentine passing through the piles with specified spacing. The test can accurately reflect the handling stability of the racing under continuous sharp turns and near-side slip conditions.

In the high-speed obstacle avoidance project in FSAE competition, the minimum pile distance is 10m, which is far less than 30m in the snake-shaped test pile distance in the



This article has been accepted for publication in a future issue of this journal, but has not been fully edited. Content may change prior to final publication.

national standard.  In order to meet the standard and achieve higher scores in the dynamic project, the pile distance is modified to 10m, and the speed is the average speed of our formula racing in the high-speed obstacle avoidance project of 45km/h. Because the distance between the snake-shaped test piles is far less than 30m specified in the national standard, the final comprehensive score of the snake-shaped test is lower than that when the pile distance is 30m.

(1) Serpentine test method

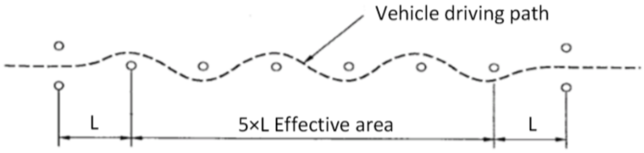


**Fig.12.** Layout of serpentine test road piles

The snake-shaped test consists of 10 stakes to form an obstacle, the stake distance L is 10m, the speed is the average speed of 45km/h in the high-speed obstacle avoidance project of Shandong University of Technology's formula racing, follow the route shown in Fig. 12 to pass through the marking area in a snake-like manner, and record the entire test process.

(2) Snake-shaped setup and simulation results

In the vehicle simulation of ADAMS/CAR, use Event Builder to set the track route and the driving events, such as steering, accelerator, braking, etc., according to the test method. The track route is set as shown in Fig. 13(a), and the simulation results of snake-shaped test are shown in Fig. 13(b)-(c).

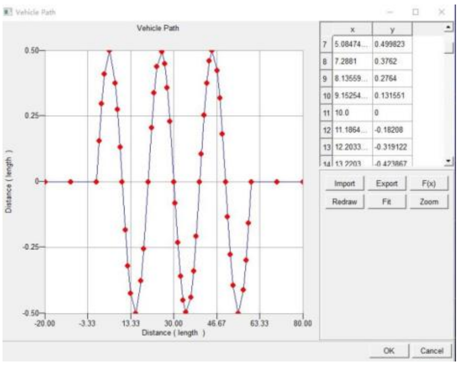


(a) Setup of snake-shaped test track route

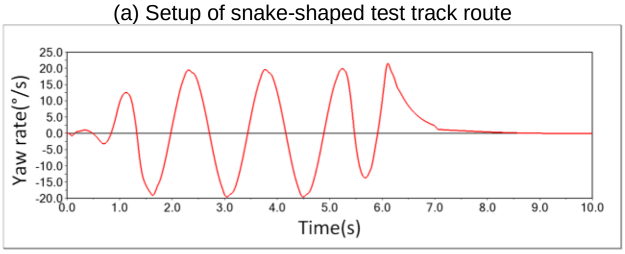


(b) Yaw rate versus time curve

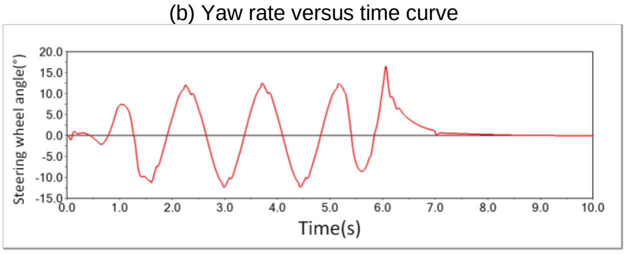


(c) Change curve of steering wheel angle with time

**Fig.13.** Simulation diagram of serpentine test

Fig. 13(c). shows that the average steering wheel angle peak θ ratio is small at 11.67 °. This is because the steering ratio of the steering system is small in racing design, and the maximum single-side steering angle of the steering wheel is only 134.6 °. This is designed to give the racing a more flexible turn and allow it to pass faster through the short track.

(3) Scoring Evaluation of Serpentine Test

Score the average yaw rate peak r and the average steering wheel peak θ at the reference speed, and finally calculate the comprehensive score.

1 Average yaw rate peak score

Calculation formula of average yaw rate peak score:

$$N_r = 60 + \frac{40}{r_{60} - r_{100}}\left(r_{60} - r\right) \tag{5}$$

$N_r$ is the average yaw rate peak evaluation score; $r$ is the test value of the average yaw rate peak; $r_{60}$ and $r_{100}$ are the lower and upper limits of the mean yaw rate peak, respectively. $r_{100}$ =10(°)/s, $r_{60}$ =25(°)/s.

From Fig. 13(b), the average yaw rate peak value $r$ is 19.01 (°)/s. Substitute each parameter into Eq. (5) to obtain the evaluation score $N_r$ =75.97 of the average yaw rate peak value of the snake-shaped test.

2 Average steering wheel angle peak score

Calculation formula of average steering wheel angle peak score:

$$N_\theta = 60 + \frac{40}{\theta_{60} - \theta_{100}}\left(\theta_{60} - \theta\right) \tag{6}$$

$N_\theta$ is the evaluation score of average steering wheel angle peak value; θ is the test value of average steering wheel angle peak value; $\theta_{60}$ and $\theta_{100}$ are the lower and upper limits of the average peak steering wheel angle, respectively. $\theta_{100}$ =60°, $\theta_{60}$ =180°.From Fig. 13(c), it can be seen that the average peak value of the steering wheel angle θ is 11.67 °. Substitute each parameter into Eq. (6), and the evaluation score of the average peak value of the steering wheel angle of snaking test $N_\theta$ =116.11.

If the evaluation score exceeds 100, the comprehensive score is calculated as 100, so $N_\theta$ =100.

3 Comprehensive Scoring of Serpentine Test

The formula for calculating the comprehensive evaluation score of snake-shaped test is:

$$N_S = \frac{2N_r + N_\theta}{3} \tag{7}$$

Substitute each parameter into Eq. (7) and the comprehensive score of the shaped test $N_S$ =83.98.

It can be seen from the simulation curve and test score of the snake-shaped test that the change range of the yaw rate is relatively small, and the stability and safety of driving can be maintained in case of sharp steering. The average peak value of the steering wheel angle is relatively small, the maneuverability of racing is good, and the steering is flexible in continuous steering. All scores meet the requirements.



This article has been accepted for publication in a future issue of this journal, but has not been fully edited. Content may change prior to final publication.

### 4.3. Comprehensive evaluation of vehicle handling stability.

The calculation formula for the objective evaluation score of manipulation stability is:

$$N = \frac{N_W + N_S}{2} \tag{8}$$

Substitute the evaluation score of each handling stability test into Eq. (8) to obtain the comprehensive evaluation score of the vehicle's handling stability as 84.04, comply with national standards. While the test difficulty is higher than the national standard, the final score is still more than 80 points, which indicates that the vehicle handling stability is good.

## 5. Verification Of Real Vehicle Test

The decoupling suspension studied in this paper is mainly used in the design and manufacture of Shandong University of Technology. A real vehicle test was conducted after the racing was manufactured to verify the relevant evaluation indicators of the snake-shaped test and the maximum lateral acceleration reflecting the ultimate lateral performance of the racing. The decoupling suspension racing is shown in Fig. 14.

This time, the test system is to read the yaw rate data through MPU-6050 gyroscope, store it in the SD card, and obtain the test process data through the computer. The test system is installed, as shown in Fig. 15.


(a)Decoupling suspension system (b)Real vehicle

**Fig.14.** Decoupling suspension racing

**Fig.15.** Installation drawing of test system

### 5.1. Snake-shaped test.

Based on the snake-shaped test method and the use of a pile barrel to form an obstacle, an experienced racer carried out a real vehicle test, and the running of the real vehicle is shown in Fig. 16.

**Fig.16.** Running of snake-shaped test

At the end of the test, the computer is used to obtain the original data and fit it to get the curve of yaw rate changing with time, as shown in Fig. 17(a).

Due to the influence of sensor error, environment, and other factors during the actual vehicle test, the signal noise will be generated, and some "burrs" will appear on the curve. To improve the effective data analysis, the yaw rate comparison curve between the real vehicle test and the virtual simulation is obtained after filtering the original data, as shown in Fig. 17(b).

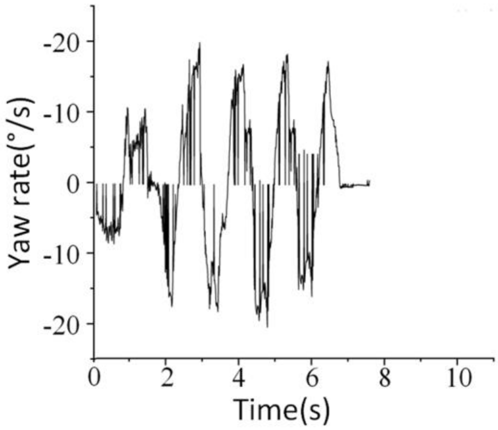


**(a) Original data of serpentine test**

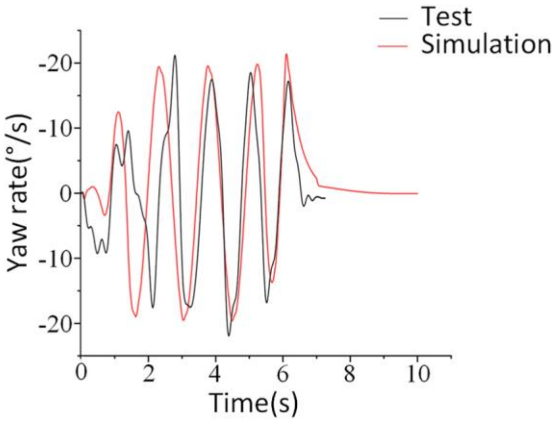


**(b) Yaw rate comparison**

**Fig.17.** Contrast curve of yaw rate between the original data of snake-shaped test and virtual simulation

From Fig. 17(b), it can be concluded that the yaw rate curve of the virtual simulation in the snake-shaped test agrees with the curve obtained by the real car running of the real racer. However, there are some errors between test and simulation caused by factors such as the long service time of the tire, assembly error, and site pavement, and the error is within the acceptable range.

The test further verifies that the handling stability of the racing is good, and the racing can have good directional stability under continuous turning conditions.

### 5.2. Maximum lateral acceleration test.

Because the racing needs a large lateral acceleration to turn quickly, keep the racing running continuously around a 9.125m radius and observe whether it can maintain a large lateral acceleration during driving. Experienced racers carry out the real car test, and the real car running is shown in Fig. 18.



This article has been accepted for publication in a future issue of this journal, but has not been fully edited. Content may change prior to final publication.

**Fig.18.** Running of real vehicle

At the end of the test, the original data is acquired by the computer, and the data after the stable driving of the racing is selected to fit and obtain the curve of lateral acceleration with time. The original fitting curve is shown in Fig. 19(a), and the filtered curve is shown in Fig. 19(b).

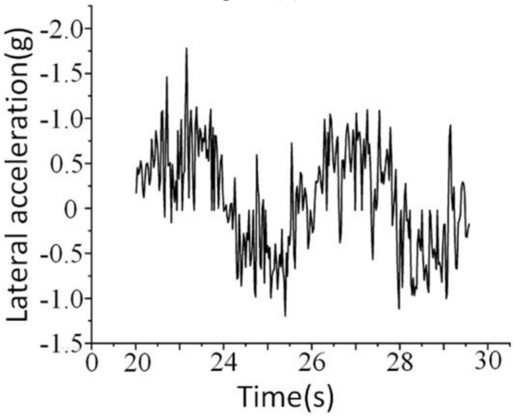


(a) Original data of lateral acceleration

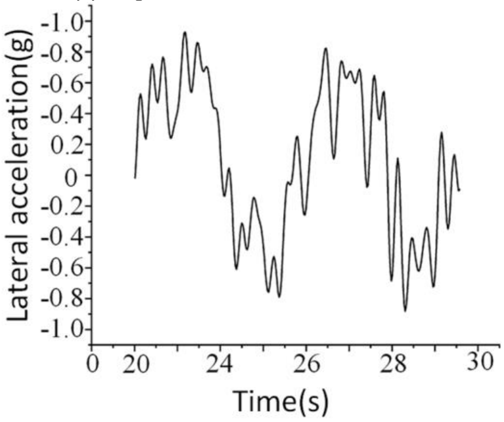


(b) Processed lateral acceleration

**Fig.19.** Curve of lateral acceleration with time

Fig. 19(b) shows that the maximum lateral acceleration of a race can reach 0.91g during continuous circular driving. This value is slightly lower than the simulation value. Still, the error is within the acceptable range, which is caused by a combination of factors such as long tire use time, assembly error, and ground surface. The ability of the racing to last for a long time, around 0.65g, suggests that the real car can maintain a large continuous lateral acceleration.

The test further verifies that the decoupling suspension system can give the vehicle a large ultimate lateral acceleration, and the riding handling stability is good.

## 6. CONCLUSIONS

In order to ensure the decoupling of suspension, a new decoupling arrangement scheme of spring damper assembly is designed in this paper. The rocker arm is transformed into a stepped shaft, and a decoupled suspension model is established. Through kinematic simulation analysis, the decoupled suspension realizes the decoupling of pitch stiffness and roll stiffness.

(1) In this paper, the maximum lateral acceleration, understeer degree and body roll degree are taken as the evaluation indicators of the test, and the test standard and difficulty are improved to evaluate the vehicle handling stability more comprehensively.

(2) The decoupling suspension was applied to Shandong University of Technology. The test was conducted in a field meeting the competition requirements. The data was read by MPU-6050 gyro test system and stored in an SD card. The test process data was obtained by a computer and fitted. In order to improve the effective analysis of data, the original data is filtered. The results show that the yaw angle velocity curve of the virtual simulation in the snake-shaped test is in good agreement with the curve obtained by the real car. The maximum lateral acceleration of the car can reach 0.91g in the continuous circular driving, slightly lower than the simulation value, and the error is within the acceptable range. It is further verified that the decoupling suspension system can make the vehicle have a large ultimate lateral acceleration, and the driving stability of the car is good.

In this paper, there is no in-depth lightweight research in the design of decoupling suspension. Therefore, topology optimization and new materials can be used in the lightweight design of uncoupled suspension, so as to further reduce the suspension mass and improve the vehicle performance.

## REFERENCES

[1] Shida Song, "Joint Study on Aerodynamics and Handling Stability of FSAE Racing Car under Unsteady Wind," M.A. thesis, Jilin Universit y, China, 2021,doi: 10.27162/d.cnki.gjlin.2021.003384

[2] Yuen T J, Foong S M, "Ramli R. Optimized suspension kinematic pro files for handling performance using 10-degree-of-freedom vehicle m odel," *Journal of Multi-body Dynamics*, vol. 228(1), pp. 82-99, 2014, doi: 10.1177/1464419313516436.

[3] Gao J, Han P, "Analysis and optimization of vehicle handling stability with considering front and rear suspension hard point coordinates," *J ournal of Mechanical Engineering Science*, vol. 236(10), pp. 5318-53 41, 2022,doi: 10.1177/09544062211060732.

[4] Ramakrisna S, Reddy B R H, Akhil B, et al. "A Review on Anti-Roll Bar used in Locomotives and Vehicles," *International Journal of Cur rent Engineering and Technology*, vol. 7(3), pp. 838-841, 2017.

[5] Zhou J, He S, "Design of third spring decoupling suspension system," *Third International Conference on Control and Intelligent Robotics ( ICCIR 2023)*, vol. 12940, pp. 244-251, 2023,doi: 10.1117/12.301114 3.

[6] Sindhwani R, Bhatnagar A, Soni A, et al. "Design and optimization of suspension for formula Society of Automotive Engineers (FSAE) veh icle," *Materials Today*, vol. 38, pp. 229-233, 2021,doi: 10.1016/j.mat pr.2020.07.077.

[7] Kumar Y, Siddiqui R A, Upadhyay Y, et al. "Kinematic and Structural Analysis of Independent type suspension system with Anti-Roll bar for Formula Student Vehicle," *Materials Today*, vol. 56, pp. 2672-2679, 2022,doi: 10.1016/j.matpr.2021.09.247.

[8] Javanshir I, Maseleno A, Tasoujian S, et al. "Optimization of suspension system of heavy off-road vehicle for stability enhancement using integrated anti-roll bar and coiling spring mechanism," *Journal of Central South University*, vol. 25(9), pp. 2289-2298, 2018,doi: 10.1007/s11771-018-3913-6.

[9] Kelkar S S, Gautam P, Sahai S, et al. "A detailed study on design, fabrication, analysis, and testing of the anti roll bar system for formula student cars," *SN Applied Sciences*, vol. 3, pp. 1-14, 2021,doi:



This article has been accepted for publication in a future issue of this journal, but has not been fully edited. Content may change prior to final publication.

10.1007/s42452-021-04279-z.

[10] Ke Ma, "Design and optimization of electric vehicle Air suspension Structure based on handling stability," M.A. thesis, Xihua University, China, 2023,doi: 10.27671/d.cnki.gcjtc.2021.000981.

[11] Liu Z, Li Z, Chen G, et al. "Suspension Design of Formula Racing Vehicle with Roll Independent Control Function," *Proceedings of China SAE Congress 2020: Selected Papers. Lecture Notes in Electrical Engineering*, vol. 769, pp. 35-56, 2022,doi: 10.1007/978-981-16-2090-4_3.

[12] Xuan Shi, Yinxin Ye, Yuhui Peng, "Pitch Motion Analysis of Front Suspension Based on The Third Spring Structure," *Auto time*, vol. 08, pp. 79-82, 2020.

[13] Shifeng Yang, Wenxuan Lu, Qianyue Tan, et al. "Optimization Analysis of a Decoupling Suspension Based on Adams," *Automobile Applied Technology*, vol. 03, pp. 49-54, 2021,doi: 10.16638/j.cnki.1671-7988.2022.003.011.

[14] Dongmei Wu, Ning Gao, Sheng Hong, et al. "Design and Simulation Research on Decoupling Suspension of FSAE Racing Car Based on ADAMS/CAR," *Journal of Wuhan University of Technology*, vol. 06, pp. 77-84, 2020.

[15] Shuanglu Quan, Shuai Wei, Fengyu Fei, et al. "Decoupled Suspension Design and Motion Simulation Analysis of Chines Formula SAE," *Automobile Applied Technology*, vol. 15, pp. 59-62, 2024,doi: 10.16638/j.cnki.1671-7988.2024.015.012.

[16] Li Y, Qing X, Zhu Y, et al. "The Application of ADAMS Software to Vehicle Handling Stability: A Review," *Performance Engineering and Maintenance Engineering*, vol. 117, pp. 785-795, 2021,doi: 10.1007/978-3-030-99075-6_63.

[17] Pridie A, Antonya C, "The theoretical study of an interconnected suspension system for a formula student car," *Applied Sciences*, vol. 11(12), pp. 5507, 2021,doi: 10.3390/app11125507.

[18] Zhang L, Liu J, Pan F, et al. "Multi-objective optimization study of vehicle suspension based on minimum time handling and stability," *Proceedings of the Institution of Mechanical Engineers. Part D, Journal of Automobile Engineering*, vol. 234(9), pp. 2355-2363, 2020,doi: 10.1177/0954407020909663

[19] Kim B M, Kim J W, Moon I D, et al. "Optimal combination of design parameters for improving the kinematics characteristics of a midsize truck through design of experiment," *Journal of Mechanical Science and Technology*, vol. 28(3), pp. 963-969, 2014,doi: 10.1007/s12206-013-1167-7.

[20] Vlad T, Alexandru C, "Multi-Criteria optimization of an innovative suspension system for race cars," *Applied Sciences*, vol. 11(9), pp. 4167, 2021,doi: 10.3390/app11094167.

[21] Zhang Z, Wang Q, Song S, et al, "Joint Research on Aerodynamic Characteristics and Handling Stability of Racing Car under Different Body Attitudes," *Energies*, vol. 15(1), pp. 393, 2022,doi: 10.3390/en15010393.

[22] Balena M, Mantriota G, Reina G, "Dynamic handling characterization and Set-Up optimization for a Formula SAE race car via Multi-Body simulation," *Machines*, vol. 9(6), pp. 126, 2021,doi: 10.3390/machines9060126.

[23] Standards of the people's Republic of China. 2014. GB/T6326-2014 Automobile Handling Stability Test Method.

[24] Standards of the people's Republic of China. 1999. QC/T 480-1999 Limits and Evaluation Methods of Automobile Handling Stability Index.

[25] Chai Y, "Simulation Optimization and Evaluation of FSAE Racing Suspension Based on Adams," M.A. thesis, North University of China, China, 2020,doi: 10.27470/d.cnki.ghbgc.2020.000790.

[26] Zhang H, "Handling Stability Optimization of FSEC Racing Suspension Based on Virtual Prototype Technology," M.A. thesis, Yangzhou University, China, 2022,doi: 10.27441/d.cnki.gyzdu.2022.000541.

[27] Zhou D, "FSAE Racing Car Layout, Suspension Design and Handling Stability Analysis," M.A. thesis, Chang'an University, China, 2013.

[28] Qiao J, Liu X, Li R, et al, "Simulation of FSAE Racing Car Control Stability," *Beijing Automotive Engineering*, vol. 4, pp. 7-9+20, 2023,doi: 10.14175/j.issn.1002-4581.2023.04.002.

[29] Yang C, "Research on Modeling and Optimal Design of Double Wishbone Front Suspension System for Baja Racing Car," M.A. thesis, Chongqing Jiaotong University, China, 2021,doi: 10.27671/d.cnki.gcjtc.2021.000981.

[30] Hong C, "Tire Model Parameter Identification and Vehicle Handling Stability Simulation Analysis of Formula Student Racing Car," M.A. thesis, Chang'an University, China, 2019.

[31] Cheng H, Wu B, He D, "Optimization Design of Suspension and Steering System for FSAE Racing Car," *Journal of Engineering Mechanics and Machinery*, vol. 8, pp. 67-81, 2023,doi: 10.23977/jemm.2023.080108.



This article has been accepted for publication in a future issue of this journal, but has not been fully edited. Content may change prior to final publication.